Supplementary Information

Confined CO in sandwich structure promotes C-C coupling in electrocatalytic CO_2 reduction

Wenya Fan,‡[a] Yinghuan Liu,‡[b] Chengbin Zhang,‡[a] Xiangdong Chen,[a] Dongpo He,[a] Mengqian Li,[a] Qing Hu,[a] Xingchen Jiao,*[a] Qingxia Chen,*[a] Yi Xie[b]

[a]Key Laboratory of Synthetic and Biological Colloids, Ministry of Education, School of Chemical and Material Engineering, Jiangnan University, Wuxi 214122, China.
[b] Hefei National Research Center for Physical Sciences at Microscale, Key Laboratory of Precision and Intelligent Chemistry, University of Science and Technology of China, Hefei 230026, China.
*Corresponding author: xcjiao@jiangnan.edu.cn; qxchen@jiangnan.edu.cn
‡These authors contributed equally to this work.

EXPERIMENTAL SECTION

Chemicals. All the chemicals were used as received without further purification. 1-Hexadecylamine (HAD, 95%) was purchased from Beijing InnoChem Science & Technology Co., Ltd. $CuCl_2 \cdot 2H_2O$, glucose anhydrous, isopropanol, chitosan (CS, Z80~95%), and acetic acid were purchased from Sinopharm Chemical Reagent Co., Ltd. Potassium hydroxide (KOH) and Nafion 117 solution (~5 wt%) were purchased from Sigma-Aldrich. Polyvinyl pyrrolidone K90 (PVP, with the average molecular weight of 300 K) and ascorbic acid were commercially available from TCI Shanghai. Hydrochloric acid (HCl), nitric acid (HNO_3), ethanol (C_2H_5OH), acetone (C_3H_6O), trichloromethane ($CHCl_3$), and N, N-dimethylformamide (DMF) were obtained from Shanghai Chemical Reagent Co., Ltd. Single layer graphene oxide powder (GO, with the diameter of 500 nm~5 μm, the thickness of 0.8~1.2 nm, and the purity of ~99%) was obtained from XFNANO. Dimethyl sulfoxide (DMSO) and deuterium oxide (D_2O) were purchased from Sigma-Aldrich. Millipore Milli-Q water (resistivity=18.2 MΩ) was used during the synthesis/assembly/characterization/electrochemical testing process.

Synthesis and purification of Cu NWs. The synthesis of Cu NWs was according to the previous report[1] with some modifications. Briefly, 5.4 g of HAD, 0.855 g of $CuCl_2 \cdot 2H_2O$ and 0.99 g of glucose were completely dissolved in 400 mL of H_2O. This homogeneous solution was placed in a 500 mL blue bottle, which was kept in water bath at 50°C with magnetic stirring for 8 h. Then the temperature was raised to 70°C and maintained for 24 h. After this, the solution was kept at 100°C for another 24 h to finish the reaction. The purification of Cu NWs was as follows with $CHCl_3$ serving as detergent[2]. 10 mL of the solution was centrifuged at 10000 rpm for 10 min. The bottom precipitation was homogeneously dispersed with 10 mL of H_2O. Subsequently, the dispersion was added into 10 mL of $CHCl_3$ and shaked vigorously following by standing for 30 min. After standing, the bottom organic layer with red sediment was centrifuged at 8000 rpm for 3 min. The centrifuged sediment was redispersed with 10 mL C_2H_5OH and 0.5 g of PVP to form a homogeneous dispersion. The mixture was stored in the refrigerator or at room temperature with moderate ascorbic acid added.

Preparation of sandwich C/Cu/C. The sandwich C/Cu/C was first prepared via a bidirectional freezing method as reported previously[3]. Briefly, chitosan powder was dispersed in 4% acetic acid with the chitosan concentration of 20 $mg \cdot mL^{-1}$. Then, moderate GO (2.7 $mg \cdot mL^{-1}$) and Cu NWs were added into the acetic acid solution of chitosan by sufficient ultrasonic treatment with the GO/Cu/CS ratio of 1:1:1. Then the uniform suspensions were poured into a PDMS mold (25.0×25.0×25.0 mm^3) with a wedge of 15° with a copper plate on the bottom. After completely frozen in liquid nitrogen for 10 min, the samples were placed into a freeze dryer (SCIENTZ-10N/C) for further freeze drying (with a vacuum degree of 5 Pa and temperature of –50 °C) for over 48 h. Finally, the obtained foams were treated in a tube furnace under N_2 gas (99.999%, purchased from Wuxi XinXiYi Technology Co., Ltd.) flow at 500 °C for 1 h with a heating rate of 2 $°C \cdot min^{-1}$ and then kept at 1000 °C for 2 h with a heating rate of 10 $°C \cdot min^{-1}$.

Material characterizations. Transmission Electron Microscopy (TEM) with Hitachi H-7650 operating at an acceleration voltage of 120 kV was used to observe the morphology of the NW and assembly. High-resolution morphological and structural features were determined with H-7700 apparatus at 100 kV. The STEM and HRTEM images, SAED, and EDX elemental mappings were taken on a JEMARM 200F atomic resolution analytical microscope with an acceleration voltage of

200 kV. Scanning electron microscopy (SEM) images were obtained with Hitachi S-4800 operating at an acceleration voltage of 30 kV. X-ray diffraction (XRD) pattern was collected on a Bruker D8 X-ray diffractometer with a Cu Kα X-ray source ($\lambda = 1.5418$ Å). Thermogravimetric analysis (TGA) was carried out on a DSC/TG synchronous thermal analyzer (Mettler Toledo, TGA2) under N_2 atmosphere with a heating rate of 10°C/min. Inductively coupled plasma spectrometry (ICP) with an Optima 7300 DV (ThermoScientific PlasmaQuad 3) was used to determine the elemental analysis of Cu in the catalysts. a. The NMR experiments were carried out on with a 400-MHz Bruker AVANCE AV III NMR spectrometer. Fourier Transform Infrared Spectroscopy (FTIR) was performed using the Thermo Scientific Nicolet iS20. Raman spectroscopy was performed on Horiba LabRAM HR Evolution. Liquid-phase products were determined and quantified by the nuclear magnetic resonance (Bruker, AVANCE Ⅲ HD 400 MHz). The gas-phase products were analyzed with the gas chromatography (GC, Agilent 8860). Flow cell was commercially available from CX (CX-Flow Cell, 10×10 mm). X-ray photoelectron spectroscopy (XPS) was recorded via a Thermo Scientific K-Alpha system, where the size of the X-ray spot was 400 mm, with an Al Kα monochromatic source. XPSPEAK 4.1 software was used for all of the XPS data processing. The X-ray absorption near edge structure (XANES) data of catalysts were obtained from the Catalysis and Surface Science Endstation at the BL11U beamline in the National Synchrotron Radiation Laboratory (NSRL) in Hefei, China. And the detailed explanation of the XANES result has also been revised.

Electrochemical measurements. The electrochemical measurements of CO_2RR were carried out in a flow cell system (CX-Flow Cell, 10 X 10 mm) on a VSP-300 Potentiostat workstation (CHI760E C23460d) with a current amplifier (CHI680D C23643). Ag/AgCl electrode (saturated in 3.0 M KCl) and Ni mesh were employed as the reference and anode electrode, respectively. Catalyst-deposited gas diffusion electrode (GDEs, YLS-30T) was used as the cathode electrode. The cation exchange membrane (Fumasep FAA-3-50) was selected to separate the cathode and anode chambers. The peristaltic pump (BT100-2J, Longer Pump) was applied to circulate the catholytes (25 mL, 1.0 M KOH) and anolytes (25 mL, 1.0 M KOH) with the flow rate of electrolytes kept at 20 mL min^{-1}. Gaseous CO_2 (99.999%, purchased from Wuxi XinXiYi Technology Co., Ltd.) was passed through the cathode chamber with a flow rate of 30 sccm monitored by a gas mass flow controller (C100L, Sierra) during the whole CO_2RR measurements. The electrochemical impedance spectroscopy (EIS) was recorded on CHI760E electrochemical workstation utilizing a three-electrode configuration in CO_2-saturated alkaline solution with a VoltaLab potentiostat (PGZ-301).

Products analysis of CO_2RR. The gas-phase products were analyzed by a gas chromatography (GC-2014, Shimadzu) equipped with a thermal conductivity detector (TCD) and a flame ionization detector (FID) to quantify H_2 and other carbon-containing products, respectively. The FEs of the gas products was calculated as bellow:

$$FE_i = \frac{q_i}{q_{total}} \times 100\% = \frac{x_i \times n \times \varphi_i \times F}{I \times t} \times 100\%$$

$$n = \frac{P \times V}{R \times T} = \frac{P \times s \times t_0}{RT}$$

$$FE_i = \frac{x_i \times P \times s \times t_0 \times \varphi_i \times F}{I \times R \times T} \times 100\% = 6.58 \times 10^{-2} \times \frac{x_i \times s \times \varphi_i}{I} \times 100\%$$

Where FE_i is the Faradaic efficiency of the gas product i; Q_i is the charges transferred during the formation of the liquid product i; Q_{total} is the total charges passing through the working electrode; x_i is the electrons transferred during the formation of the liquid product i; n is the total molar content of the gas product; φ_i is the volume fraction of the gas product i determined by GC; s is the outflow rate; t_0 is the gas injection time of 1.0 s; t is the CO_2RR time of 10 min; F is the Faradaic constant of 96,485 C·mol^{-1}; I is the total current during CO_2RR; V_m is the gas molar volume at room temperature of 24.5 L·mol^{-1}.

Liquid-phase products were determined and quantified by ^{1}H NMR spectra on Agilent 600 MHz DirectDrive2 spectrometers under water suppression mode. Typically, the internal standard solution was prepared by mixing 100 μL of D_2O and DMSO with DMSO concentration of 50 ppm. Then, this internal standard solution was added into 500 μL of catholyte diluted from 1.0 M KOH to 0.01M. The FEs of the liquid products was calculated as bellow:

$$FE_i = \frac{q_i}{q_{total}} \times 100\% = \frac{x_i \times n_i \times F}{I \times t}$$

$$\frac{{}^{s_{DMSO}}/_{6}}{{}^{s_i}/_{y_i}} = \frac{c_{DMSO} \times 20 \times 10^{-3}}{n_i \times {}^{0.0004}/_{0.1}}$$

$$c_{DMSO} = \frac{\rho_{DMSO}}{M_{DMSO}} \times 10^{-4} = \frac{1.1}{78.13} \times 10^{-4} = 1.41 \times 10^{-6} (mol\ mL^{-1})$$

$$n_i = 4.23 \times 10^{-5} \times \frac{s_i}{s_{DMSO} \times y_i}$$

$$FE_i = \frac{x_i \times 4.23 \times 10^{-5} \times \frac{s_i}{s_{DMSO} \times y_i} \times F}{I \times t} \times 100\% = 6.8 \times 10^{-3} \times \frac{x_i \times s_i}{y_i \times I} \times 100\%$$

Where FE_i is the Faradaic efficiency of the liquid product i; Q_i is the charges transferred during the formation of the liquid product i; Q_{total} is the total charges passing through the working electrode; x_i is the electrons transferred during the formation of the liquid product i; n_i is the molar content of the liquid product i in the catholyte determined by NMR; F is the Faradaic constant of 96,485 C·mol^{-1}; I is the total current during CO_2RR; t is the CO_2RR time of 10 min; s_{DMSO} and s_i are the peak area of DMSO and the liquid product i in NMR, respectively; c_{DMSO} is the concentration of DMSO used before NMR preparation; y_i is the proton of the liquid product i; ρ_{DMSO} and M_{DMSO} are the density and molar mass of DMSO.

Kinetic simulation details. The sandwich C/Cu/C system in this study consists of a Cu catalyst layer in the middle of two rGO nanosheets, while the C/Cu mixture system consists of a Cu catalyst layer on one rGO nanosheet. The sizes of the Cu catalyst layer and rGO nanosheets in these two systems remain the same. Chemical species including the products of electrocatalytic CO_2RR, such as CO, CH_4, C_2H_4, C_2H_5OH, and AcOH in the solution, and the key intermediates, such as COH^*, CHO^*, CH_2^*, CH_2CO^*, $C_2O_2^*$, $C_2O_2H^*$, CH_2CHO^*, CH_3CHO^*, and $C_2H_5O^*$ are considered. The kinetic factors consist of the diffusion of CO_2, CO and different products in the solution, the adsorption/desorption of CO ($CO + * \leftrightarrow CO^*$), and the electron transfer on catalysts, which includes the conversion of CO_2 in solution into the adsorbed CO (CO^*), conversion of CO^*

via the pathway of $CO^* - CO^*$ dimerization into C_2 and the pathway of C_1 production. The detailed reaction processes can be written as follows[4, 5].

$$CO_2 + 2e^- + 2H^+ + * \rightarrow CO^* + H_2O$$

$$CO^* \rightarrow CO + *$$

$$CO^* + H^+ + e^- \rightarrow COH^*$$

$$COH^* + 5H^+ + 5e^- \rightarrow CH_4 + H_2O$$

$$COH^* + 3H^+ + 3e^- \rightarrow CH_2^* + H_2O$$

$$CH_2^* + CO \rightarrow CH_2CO^*$$

$$CH_2CO^* + OH^- \rightarrow CH_3COO^-$$

$$CO^* + H^+ + e^- \rightarrow CHO^*$$

$$CHO^* + 5H^+ + 5e^- \rightarrow CH_4$$

$$2CO^* + e^- \rightarrow C_2O_2^{-*}$$

$$C_2O_2^{-*} + H^+ \rightarrow C_2O_2H$$

$$C_2O_2H + 5H^+ + 5e^- \rightarrow C_2H_4 + H_2O$$

$$C_2O_2H + 4H^+ + 4e^- \rightarrow CH_2CHO^* + H_2O$$

$$CH_2CHO^* + H^+ + e^- \rightarrow CH_3CHO^*$$

$$CH_3CHO^* + H^+ + e^- \rightarrow CH_3CH_2O^*$$

$$CH_3CH_2O^* + H^+ + e^- \rightarrow CH_3CH_2OH$$

The above kinetic processes are performed on the Cu catalyst layer and in the solution nearby the electrode surface. The two-dimensional system under study was discretized into a N × N rectangular grid for simulation shown as bellow. Therefore, the diffusion in solution at position $\mathbf{r}$ can be modeled by the following diffusion equations[6].

$$\frac{\partial c_{CO_2}(\mathbf{r})}{\partial t} = D_{CO_2}\nabla^2 c_{CO_2}(\mathbf{r})$$

$$\frac{\partial c_{CO}(\mathbf{r})}{\partial t} = D_{CO}\nabla^2 c_{CO}(\mathbf{r})$$

$$\frac{\partial c_{AcOH}}{\partial t} = D_{EtOH}\nabla^2 c_{AcOH}(\mathbf{r})$$

$$\frac{\partial c_{CH_4}}{\partial t} = D_{CH_4}\nabla^2 c_{CH_4}(\mathbf{r})$$

$$\frac{\partial c_{C_2H_4}}{\partial t} = D_{C_2H_4}\nabla^2 c_{C_2H_4}(\mathbf{r})$$

$$\frac{\partial c_{C_2H_5OH}}{\partial t} = D_{C_2H_5OH}\nabla^2 c_{C_2H_5OH}(\mathbf{r})$$

Similarly, the above kinetic factors can be modeled on the catalyst surface with the following reaction-diffusion equations:

$$\frac{\partial c_{CO}(\mathbf{r})}{\partial t} = D_{CO}\nabla^2 c_{CO} - k_{ad,CO}c_{CO}(\mathbf{r})\left(1 - \theta_{CO}(\mathbf{r}) - \theta_{C_2}(\mathbf{r})\right) + k_{de,CO}c_{CO}(\mathbf{r})$$

$$\frac{\partial c_{C_2H_5OH}(\mathbf{r})}{\partial t} = D_{C_2H_5OH}\nabla^2 c_{C_2H_5OH} + k_{C_2H_5OH}c_{C_2H_5OH}(\mathbf{r})$$

$$\frac{\partial c_{C_2H_4}(\mathbf{r})}{\partial t} = D_{C_2H_4}\nabla^2 c_{C_2H_4} + k_{C_2H_4}c_{C_2H_4}(\mathbf{r})$$

$$\frac{\partial c_{AcOH}(\mathbf{r})}{\partial t} = D_{EtOH}\nabla^2 c_{AcOH} + k_{AcOH}c_{AcOH}(\mathbf{r})$$

$$\frac{\partial c_{CH_4}(\mathbf{r})}{\partial t} = D_{CH_4}\nabla^2 c_{CH_4} + k_{CH_4}c_{CH_4}(\mathbf{r})$$

$$\frac{\partial \theta_{CO}(\mathbf{r})}{\partial t} = k_{ad,CO_{ad}}c_{C_{CO}}(\mathbf{r})\left(1 - \sum\nolimits_{ad\ species}\theta_{ad\ species}(\mathbf{r})\right) - k_{de,CO_{ad}}\theta_{CO}(\mathbf{r}) + k_{CO}c_{CO_2}(\mathbf{r})\left(1 - \sum\nolimits_{ad\ species}\theta_{ad\ species}(\mathbf{r})\right) - k_{COH}\theta_{COH}(\mathbf{r}) - k_{CHO}\theta_{CHO}(\mathbf{r}) - 2k_{C2O2}\theta_{CO}^2(\mathbf{r})$$

$$\frac{\partial \theta_{COH}(\mathbf{r})}{\partial t} = k_{COH}\theta_{CO}(\mathbf{r}) - k_{CH4}\theta_{COH}(\mathbf{r}) - k_{CH_2}\theta_{COH}(\mathbf{r})$$

$$\frac{\partial \theta_{CH_2}(\mathbf{r})}{\partial t} = k_{CH_2}\theta_{CH_2}(\mathbf{r}) - k_{CH2CO}\theta_{CH_2}(\mathbf{r})\theta_{CO}(\mathbf{r})$$

$$\frac{\partial \theta_{CH_2CO}(\mathbf{r})}{\partial t} = k_{CH_2CO}\theta_{CH_2}(\mathbf{r})\theta_{CO}(\mathbf{r}) - k_{AcOH}\theta_{CH_2CO}(\mathbf{r})$$

$$\frac{\partial \theta_{CHO}(\mathbf{r})}{\partial t} = k_{CHO}\theta_{CO}(\mathbf{r}) - k_{CH_4P2}\theta_{CHO}(\mathbf{r})$$

$$\frac{\partial \theta_{C_2O_2}(\mathbf{r})}{\partial t} = k_{C_2O_2}\theta_{CO}^2(\mathbf{r}) - k_{C_2O_2H}\theta_{C_2O_2}(\mathbf{r})$$

$$\frac{\partial \theta_{C_2O_2H}(\mathbf{r})}{\partial t} = k_{C_2O_2H}\theta_{C_2O_2}(\mathbf{r}) - k_{CH_2CHO}\theta_{C_2O_2H}(\mathbf{r})$$

$$\frac{\partial \theta_{CH_2CHO}(\mathbf{r})}{\partial t} = k_{CH_2CHO}\theta_{C_2O_2H}(\mathbf{r}) - k_{C_2H_4}\theta_{C_2O_2H}(\mathbf{r}) - k_{CH_3CHO}\theta_{CH_2CHO}$$

$$\frac{\partial \theta_{CH_3CHO}(\mathbf{r})}{\partial t} = k_{CH_3CHO}\theta_{CH_2CHO}(\mathbf{r}) - k_{C_2H_5O}\theta_{CH_3CHO}(\mathbf{r})$$

$$\frac{\partial \theta_{C_2H_5O}(\mathbf{r})}{\partial t} = k_{C_2H_5O}\theta_{CH_3CHO}(\mathbf{r}) - k_{C_2H_5OH}\theta_{C_2H_5O}(\mathbf{r})$$

Where the parameters with subscript CO_2, CO, CH_4, C_2H_4, C_2H_5OH, $AcOH$ denote those for the corresponding chemical species in the solution or adsorbed on the catalyst surface. c is the concentration of species in the solution, θ is the surface concentration of adsorbed species on the catalyst surface. D is the diffusion constant of the chemical species. k_{ad} and k_{de} are the adsorption and desorption constants of chemical species in the solution and adsorbed species on the catalyst surface. k_i is the reaction rate constant of the production of the chemical species, i is under the overpotential of η.

The energy barrier factors and the experimental results of the above reactions are combined to determine the parameters as shown in Table S1[7]. Those parameters are normalized by dimensionless units $0.86D_{CO}$, L_0 and k_BT, where L_0 is the length of the whole lattice, k_B is the Boltzmann constant, and T is the temperature, respectively.

Supplementary Figures

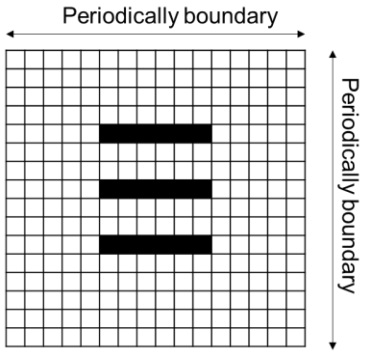

Figure S1. Periodically boundary for simulation.

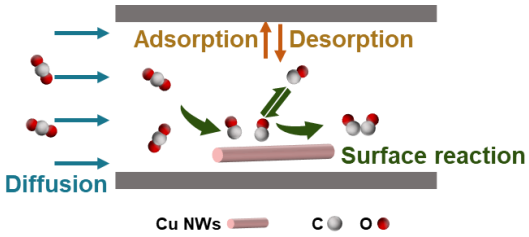

Figure S2. Kinetic process of sandwich structure for CO_2RR.

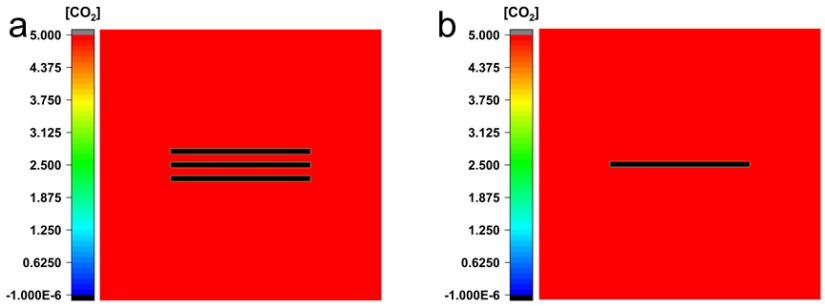

Figure S3. Simulated CO_2 concentration distributions in the sandwich structure (a) and disordered mixture (b).

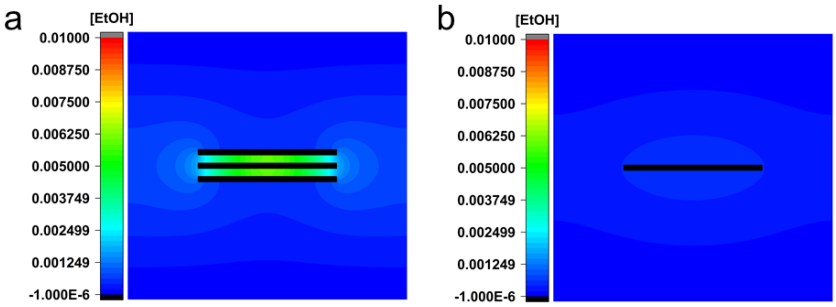

Figure S4. Simulated EtOH concentration distributions in the sandwich structure (a) and disordered mixture (b).

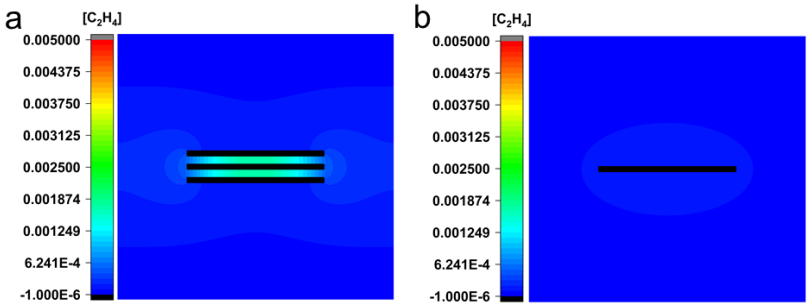

Figure S5. Simulated C_2H_4 product concentration distributions in the sandwich structure (a) and disordered mixture (b).

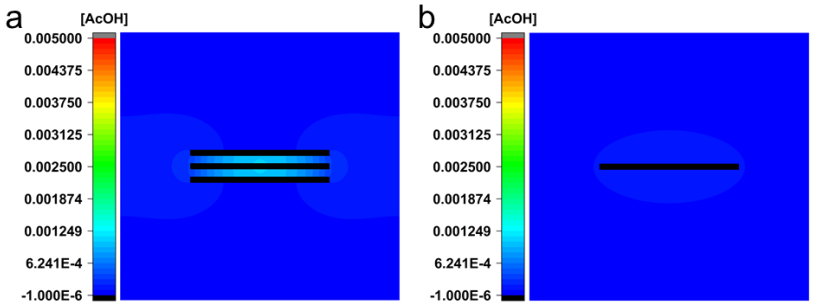

Figure S6. Simulated AcOH product concentration distributions in the sandwich structure (a) and disordered mixture (b).

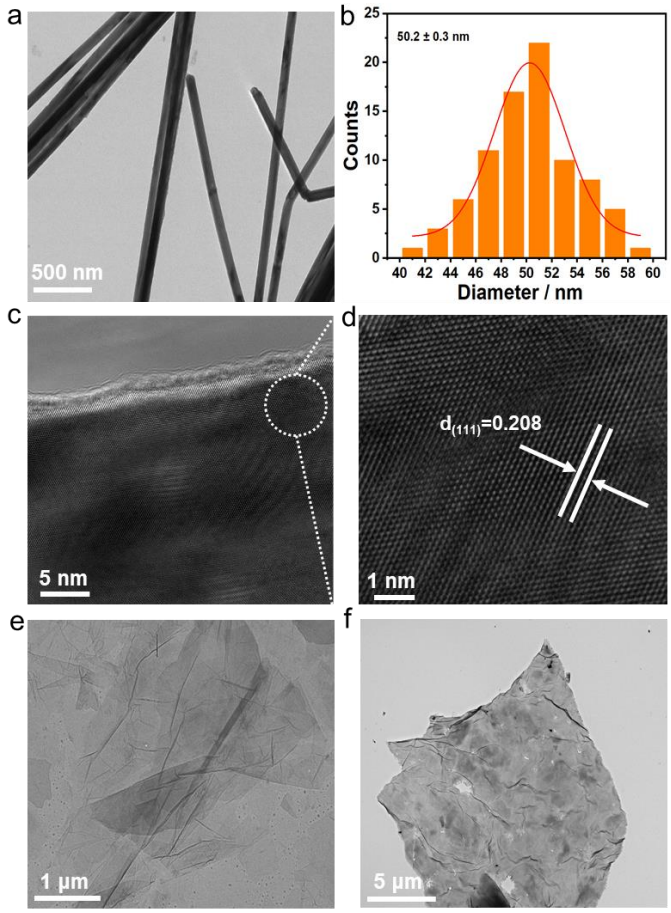

Figure S7. Morphological and structural characterizations of Cu NWs, GO, and rGO. (a) TEM image of Cu NWs. (b) Diameter distribution of Cu NWs. (c-d) HRTEM images of Cu NWs. (e) TEM image of GO. (f) TEM image of rGO.

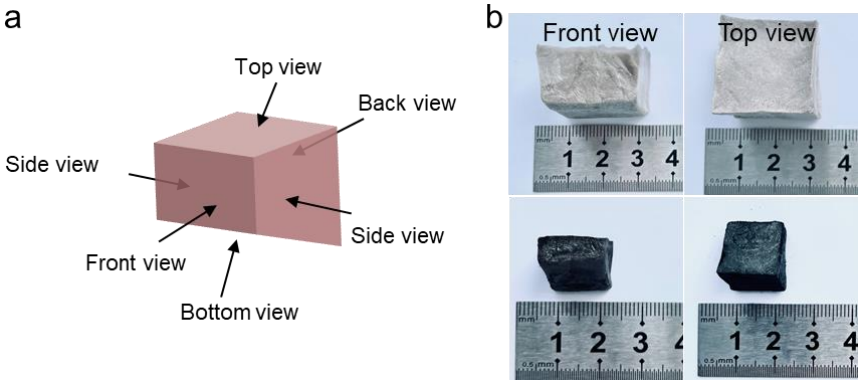

Figure S8. Schematic diagram and optical photographs of sandwich C/Cu/C before and after annealing. (a) Schematic diagram. (b) Optical photographs.

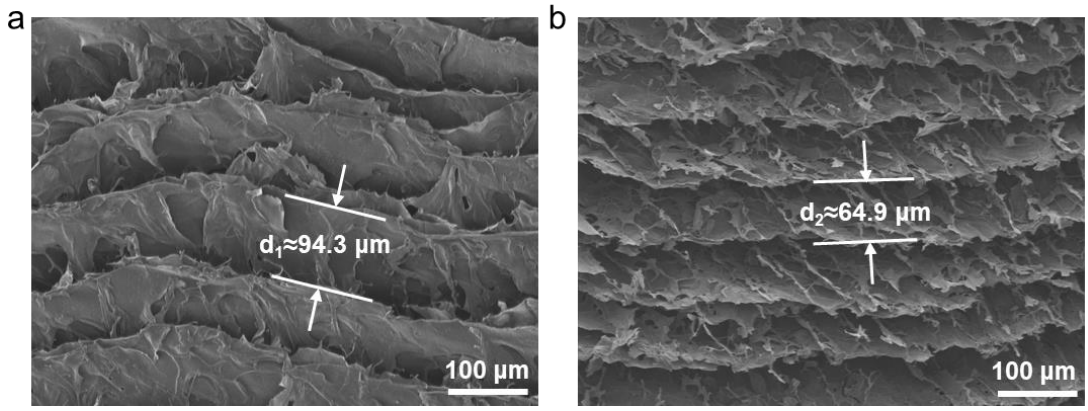

Figure S9. SEM images of sandwich C/Cu/C before and after thermal annealing.

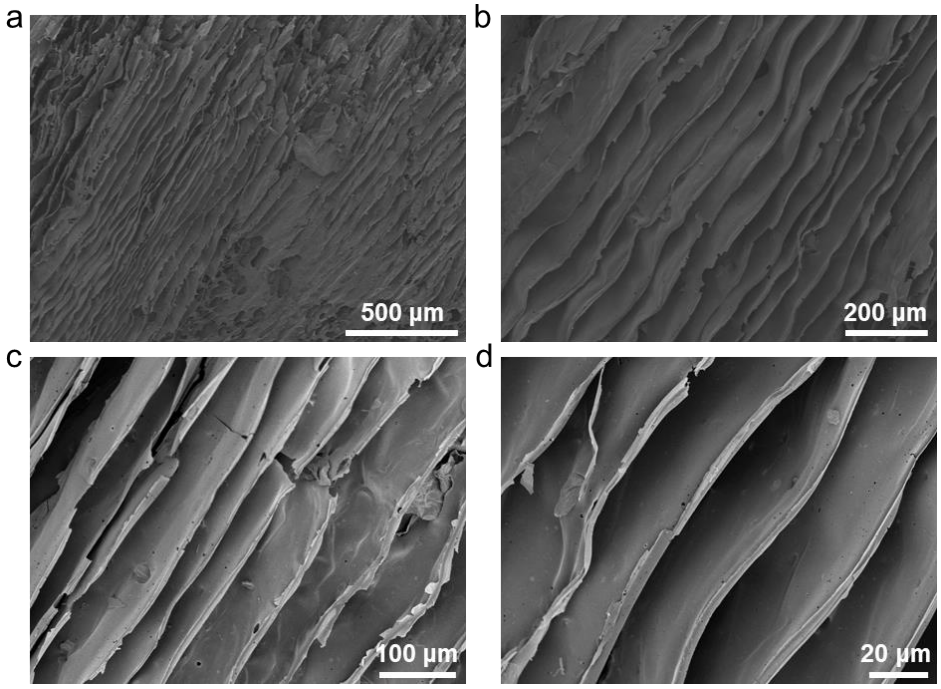

Figure S10. SEM images of sandwich C/Cu/C with different magnifications.

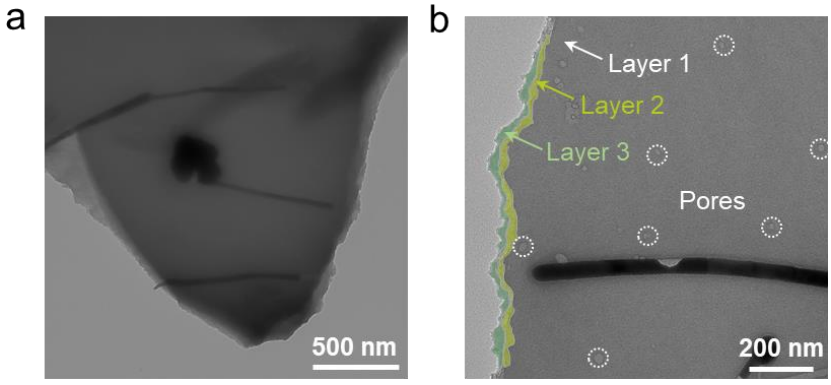

Figure S11. TEM images of sandwich C/Cu/C with different magnifications.

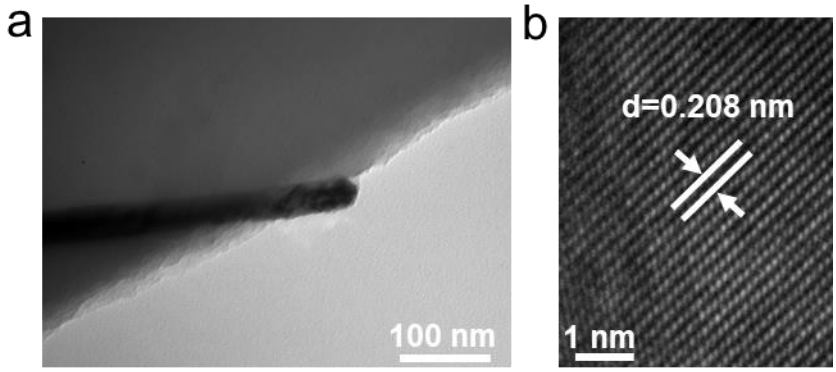

Figure S12. TEM and HTREM images of sandwich C/Cu/C.

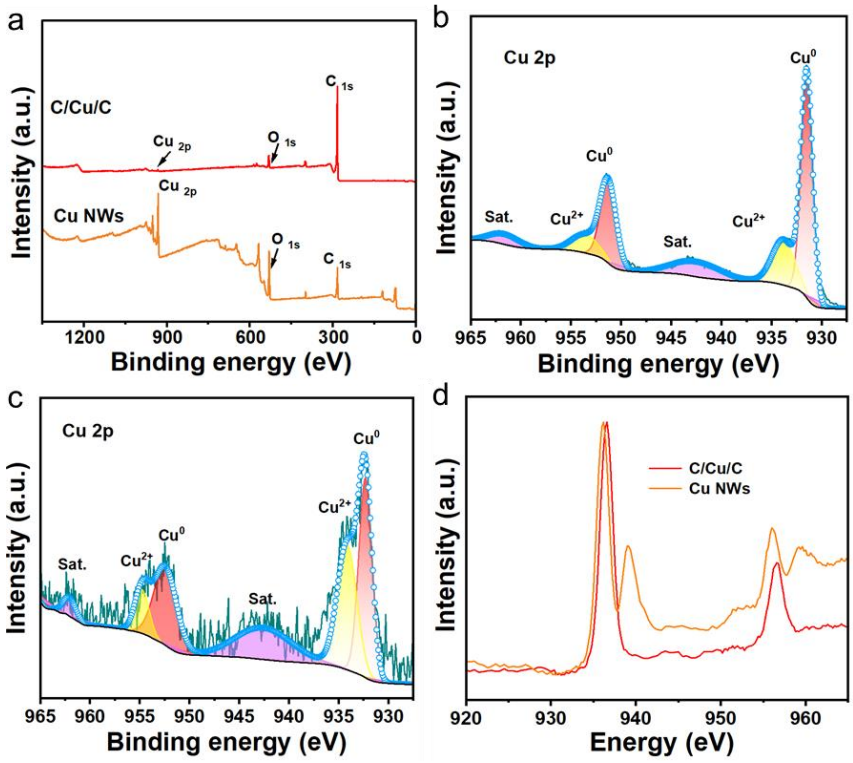

Figure S13. (a) XPS survey spectra of sandwich C/Cu/C and Cu NWs. (b-c) Cu 2p orbital XPS spectra of Cu NWs (b) and sandwich C/Cu/C (c). (d) XANES spectra of sandwich C/Cu/C and pure Cu NWs.

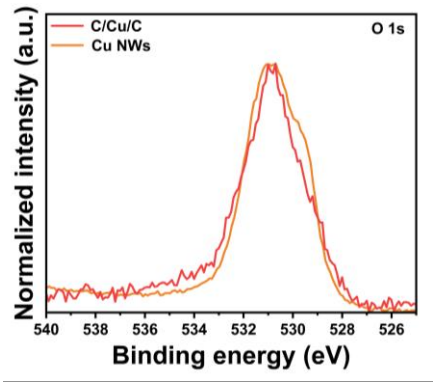

Figure S14. O 1s XPS spectra of C/Cu/C and Cu NWs.

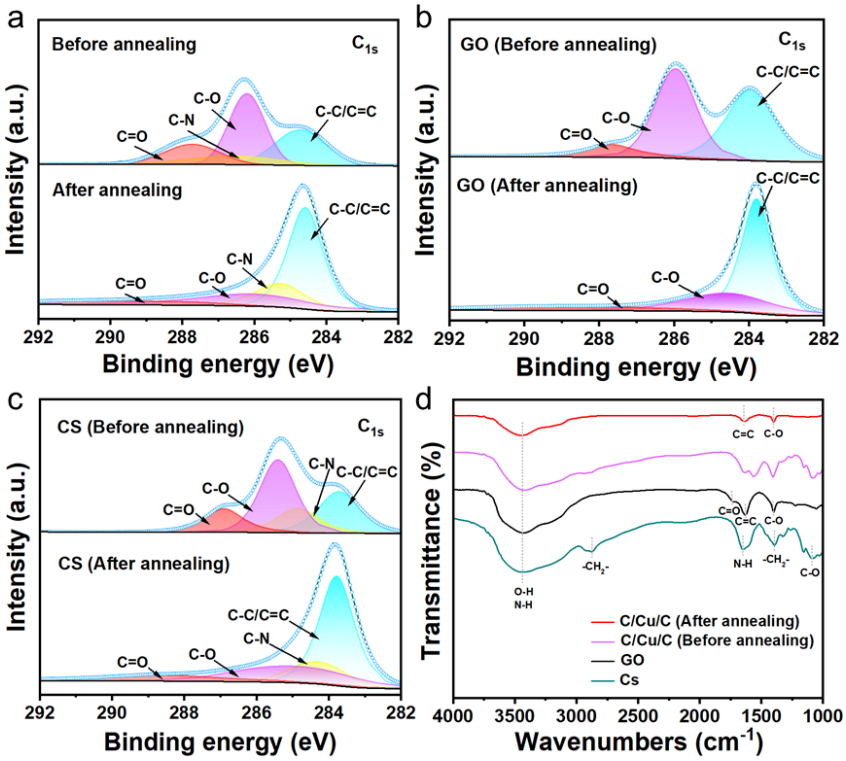

Figure S15. (a) XPS C 1s orbital spectra of sandwich C/Cu/C before and after annealing. (b-c) XPS C 1s orbital spectra of GO (b) and CS (c) before and after thermal annealing. (d) FTIR spectra of sandwich C/Cu/C before and after thermal annealing, CS, and GO.

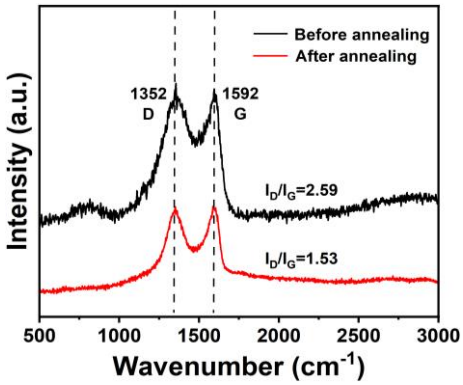

Figure S16. Raman spectra of sandwich C/Cu/C before and after annealing.

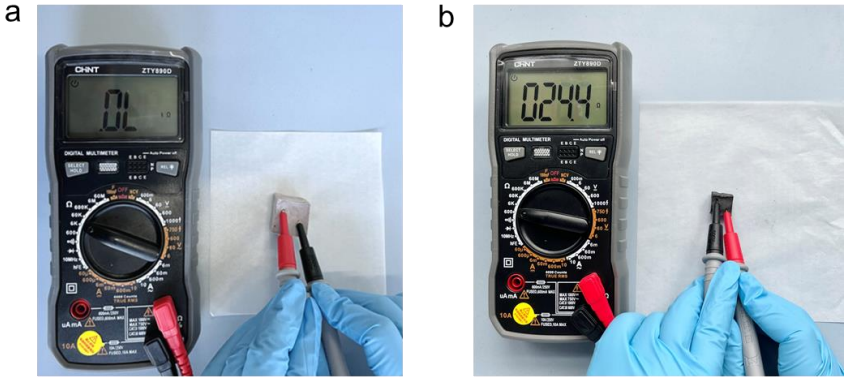

Figure S17. Optical photos of resistance testing for sandwich C/Cu/C before and after annealing.

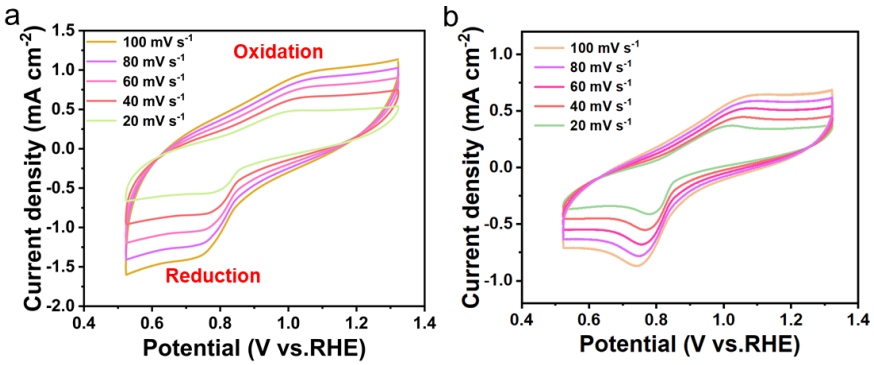

Figure S18. CV profiles at different scanning rate of sandwich C/Cu/C(a) and Cu/C mixture(b) in 1M KOH electrolyte.

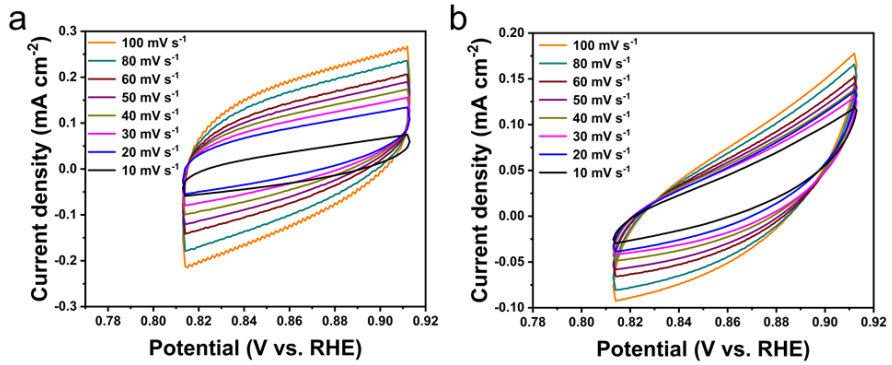

Figure S19. Cyclic voltammetry curves for (a) C/Cu/C, (b) Cu/C with the scan rates from 10 mV/s to 100 mV/s in 1M KOH electrolyte.

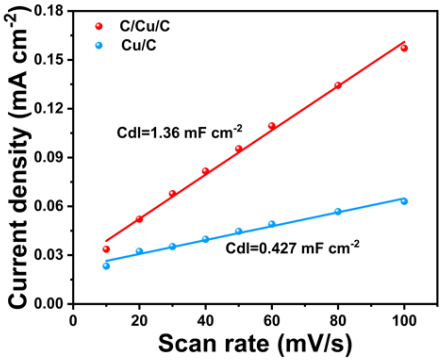

Figure S20. Electrocatalytically active surface areas (ECSA) obtained by double layer capacitance method.

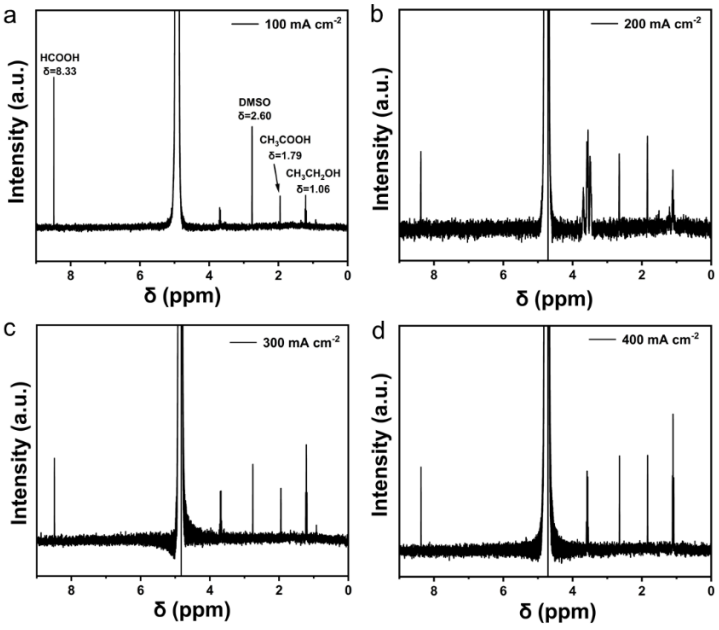

Figure S21. The corresponding ^{1}H NMR products of Sandwich C/Cu/C at different current density.

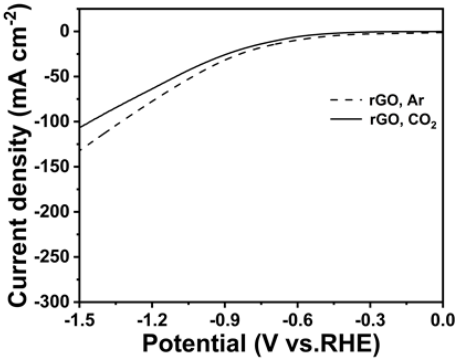

Figure S22. Current-voltage curves obtained from LSV scans. The scan rate was 10 mV s^{-1}.

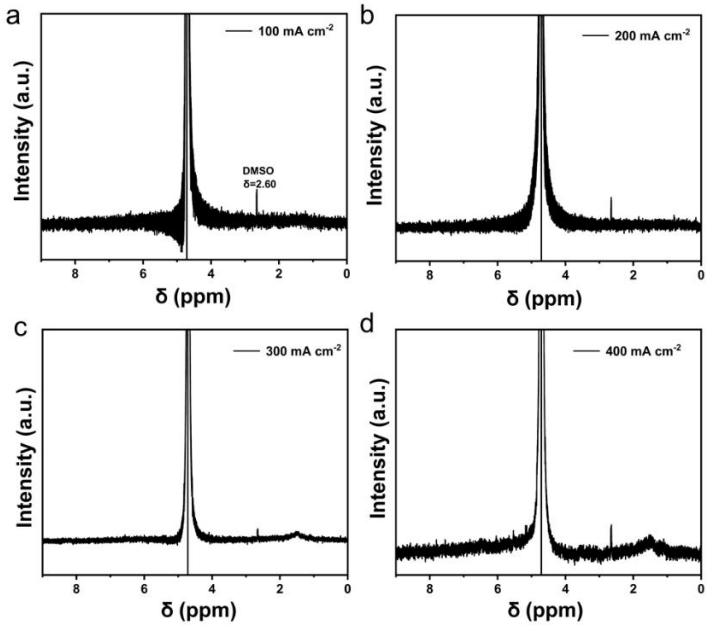

Figure S23. The ^{1}H NMR spectra of rGO at various current densities.

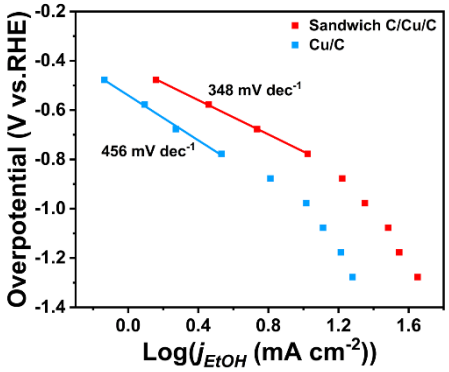

Figure S24. Tafel slope of Sandwich C/Cu/C and Cu/C.

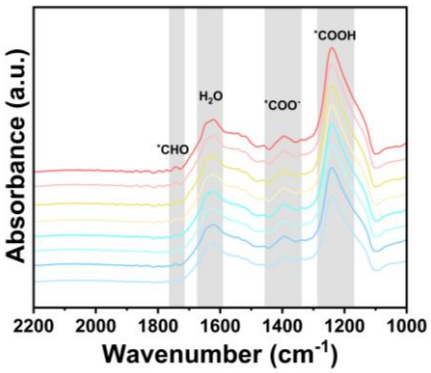

Figure S25. Electrochemical in situ FTIR spectra of Cu/C (-1.4 V vs RHE) mixture from 0 to 300 s.

Table S1. Kinetic parameters.

Parameters	D_{CO_2}	D_{CO}	D_{CH_4}	$D_{C_2H_4}$
Value	0.74	1.16	2.0	1.16
Parameters	$D_{C_2H_5OH}$	D_{AcOH}	k_{CO}	$k_{ad,CO}$
Value	1.16	1.16	0.002	0.25
Parameters	$k_{de,CO}$	k_{COH}	k_{CH4}	k_{CH2}
Value	0.35	0.0015	38.0	123.0
Parameters	k_{CH2CO}	k_{AcOH}	k_{CHO}	k_{CH4}
Value	130.0	184.0	0.002	180.0
Parameters	k_{C2O2}	k_{C2O2H}	k_{CH2CHO}	k_{C2H4}
Value	0.08	100.0	148.0	60.0
Parameters	k_{CH_3CHO}	k_{C2H5O}	k_{C2H5OH}	N
Value	200.0	92.0	88.0	400

References

1. Q. Q. Fu, Y. D. Li, H. H. Li, L. Xu, Z. H. Wang and S. H. Yu, *Langmuir*, 2019, **35**, 4364-4369.
2. F. Qian, P. C. Lan, T. Olson, C. Zhu, E. B. Duoss, C. M. Spadaccini and T. Y. J. Han, *Chem. Commun.*, 2016, **52**, 11627-11630.
3. H. L. Gao, Z. Y. Wang, C. Cui, J. Z. Bao, Y. B. Zhu, J. Xia, S. M. Wen, H. A. Wu and S. H. Yu, *Adv. Mater.*, 2021, **33**, 2102724.
4. R. Kortlever, J. Shen, K. J. P. Schouten, F. Calle-Vallejo and M. T. M. Koper, *J. Phys. Chem. Lett.*, 2015, **6**, 4073-4082.
5. R. B. Sandberg, J. H. Montoya, K. Chan and J. K. Norskov, *Surf. Sci.*, 2016, **654**, 56-62.
6. C. H. Lin and R. G. Compton, *Curr. Opin. Electrochem.*, 2019, **14**, 186-199.
7. P. Q. Ling, Y. H. Liu, Z. Q. Wang, L. Li, J. Hu, J. F. Zhu, W. S. Yan, H. J. Jiang, Z. H. Hou, Y. F. Sun and Y. Xie, *Nano Lett.*, 2022, **22**, 2988-2994.